Journal of Solid State Chemistry **168,** 331–342 (2002)
doi:10.1006/jssc.2002.9718

Structure and Properties of Gd*T*Mg (*T*=Pd, Ag, Pt)

Kazimierz Łątka* and Zbigniew Tomkowicz*

*Marian Smoluchowski Institute of Physics, Jagiellonian University, Reymonta 4, 30-059 Kraków, Poland
E-mail: uflatka@cyf-kr.edu.pl

Roman Kmieć† and Andrzej W. Pacyna†

†Henryk Niewodniczański Institute of Nuclear Physics, Radzikowskiego 152, 31-342 Kraków, Poland

Ratikanta Mishra‡

‡Applied Chemistry Division, Bhabha Atomic Research Centre, Trombay, Mumbai-400 085, India

Thomas Fickenscher§, Rolf-Dieter Hoffmann§, and Rainer Pöttgen§,[1]

§Institut für Anorganische und Analytische Chemie, Universität Münster, Wilhelm-Klemm-Straße 8, D-48149 Münster, Germany
E-mail: pottgen@uni-muenster.de

and

Holger Piotrowski¶

¶Department Chemie, Ludwig-Maximilians-Universität München, Butenandtstrasse 5–13 (Haus D), D-81377 München, Germany

Received April 12, 2002; in revised form July 2, 2002; accepted July 16, 2002

The title compounds were prepared by reacting the elements in sealed tantalum tubes in a water-cooled sample chamber in a high-frequency furnace. X-ray powder and single-crystal investigations showed isotypism with the ZrNiAl type, space group $P\tilde{6}2m$: $a = 750.1(1)$ pm, $c = 404.10(4)$ pm, w$R2 = 0.0703$, 250 F^2 values, 14 parameters for GdPdMg, $a = 768.0(2)$ pm, $c = 419.92(9)$ pm, w$R2 = 0.0579$, 261 F^2 values, 16 parameters for GdAgMg, and $a = 738.0(1)$ pm, $c = 409.02(5)$ pm, w$R2 = 0.0742$, 244 F^2 values, 14 parameters for GdPtMg. The structures contain two crystallographically different transition metal (T) sites which both have a tricapped trigonal prismatic coordination: [T(1)Gd_6Mg_3] and [T(2)Mg_6Gd_3]. Together the transition metal and magnesium atoms build three-dimensional networks in which the gadolinium atoms fill distorted hexagonal channels. The magnesium position of the silver compound shows a small degree of magnesium/silver mixing resulting in the composition $GdAg_{1.06(1)}Mg_{0.94(1)}$ for the crystal investigated. The magnetic properties of all compounds were investigated using AC and DC susceptibility as well as ^{155}Gd Mössbauer spectroscopy measurements. All investigated materials show irreversibilities between field cooled and zero-field-cooled DC magnetizations and magnetic hysteresis behavior as is typical for ferromagnets. The remanent magnetizations and coercive fields are relatively small. The Curie temperatures were determined from inflection points of the experimental susceptibilities. Additional anomalies below the ferromagnetic transitions suggest spin-reorientation processes. © 2002 Elsevier Science (USA)

Key Words: **intermetallic gadolinium compounds; crystal structure; magnetism; ^{155}Gd Mössbauer spectroscopy.**

INTRODUCTION

Today more than 1300 equiatomic intermetallic compounds *RTX* where *R* is a rare earth or an alkaline earth metal, *T* a transition metal, and *X* an element of the third, fourth, or fifth main group are known (1–6). These intermetallics crystallize with more than 40 different structure types (7). Most of them are related by group–subgroup relationships (6).

Recent studies have shown, that the *X* position in various intermetallic *RETX* compounds (*RE*=rare earth element) can completely be substituted by magnesium or

[1] To whom correspondence should be addressed.

0022-4596/02 $35.00

cadmium [(8–13) and references therein]. This way it is possible to reduce the electron count of such compounds and influence the physical properties. So far, two different structure types have been observed for such intermetallics. The *RET*Mg compounds with a trivalent rare earth atom crystallize with the hexagonal ZrNiAl-type structure (14–16), while those with the divalent rare earths, i.e., europium and ytterbium, adopt the orthorhombic TiNiSi type (17).

First property investigations showed stable trivalent cerium in CePdMg (9). No magnetic ordering was observed down to 2 K. In contrast, comparatively high Curie temperatures of 28 and 62 K have been observed for EuAuCd (12) and GdPdCd (18), respectively. Also the compounds Gd*TX* (X = Al, Ga, In) (19) with ZrNiAl or $MgCu_2$ structure might be discussed in this context. While GdMgIn remains paramagnetic down to 3 K, antiferromagnetic ordering is detected for GdMgGa at 15.3 K and ferromagnetic ordering for GdMgAl at 59 K.

Now we have concentrated our investigations on the *RET*Mg compounds with gadolinium as rare earth metal component. Such gadolinium intermetallics are of interest because of their potential use as magnetic refrigeration materials (20–22). Herein we report on the syntheses, structure determination and physical properties of Gd*T*Mg (T = Pd, Ag, Pt). Lattice parameters of the palladium and silver compounds have previously been reported by Iandelli (8).

AC and DC temperature dependencies of the magnetic susceptibilities have been undertaken in order to elucidate magnetic properties of the three compounds. Complex AC susceptibility ($\chi = \chi' - i\chi''$) measurements are a very accurate technique for the determination of magnetic-phase transitions and dynamics. In addition, studies of higher harmonics can provide valuable information on the nature of the magnetic states. On the other hand, complementary DC measurements give deeper insights into the irreversible transitions of the different magnetic phases.

Since the Gd^{3+} ion has spherically symmetric 4*f* orbitals, gadolinium-based intermetallics usually show negligible magnetocrystalline anisotropy. Due to the anisotropic gadolinium neighborhood of the Gd^{3+} ions, the magnetic centers may interact in a rather complex manner. Hence, systematic studies of such materials can shed new light on the various magnetic structures and magnetic-phase transformations.

In the present paper, ^{155}Gd Mössbauer spectroscopy is used to monitor the magnetic gadolinium substructure in order to draw some conclusions concerning possible orientations of magnetic moments with respect to the principal axes of the electric field gradient (EFG) tensor.

EXPERIMENTAL

Starting materials for the synthesis of Gd*T*Mg (T = Pd, Ag, Pt) were ingots of gadolinium (Johnson Matthey, > 99.9%), palladium and platinum powder (Degussa-Hüls, 200 mesh, > 99.9%), silver wire (Degussa-Hüls, ∅ 1 mm, > 99.9%), and a magnesium rod (Johnson Matthey, ∅ 16 mm, > 99.5%). The gadolinium ingots were first cut into smaller pieces and arc-melted to small buttons (ca. 500 mg) under an argon pressure of about 600 mbar. The argon was purified before use over molecular sieves, silica gel, and titanium sponge (900 K). The gadolinium buttons were subsequently mixed with the palladium (platinum) powder (pieces of the silver wire) and pieces of the magnesium rod in the ideal 1:1:1 atomic ratio and sealed in small tantalum tubes (about 1 cm^3) under an argon pressure of about 800 mbar. Details about the arc-welding equipment are given elsewhere (23).

The tantalum tubes were then placed in a water-cooled quartz glass sample chamber of a high-frequency furnace (KONTRON Roto-Melt, 1.2 kW) under flowing argon (24). The tubes were first heated for 1 min with the maximum power output (about 1500 K) and subsequently annealed at about 900 K for another 2 h. The tubes were finally quenched by radiative heat loss within the water-cooled sample chamber. The light-gray samples could readily be separated from the tantalum tubes after the annealing procedures. No reaction of the samples with the tubes could be detected. GdPdMg, GdAgMg, and GdPtMg are stable in moist air in the form of compact buttons as well as fine-grained powders. Single crystals exhibit metallic luster.

The samples were routinely characterized by X-ray powder patterns (Stoe StadiP) using Cu$K\alpha_1$ radiation and silicon (a = 543.07 pm) as an external standard. The lattice parameters (Table 1) were obtained by least-squares fits of the powder data. The indexing of the diffraction lines was facilitated by intensity calculations (25) using the positional parameters of the refined structures. The lattice parameters determined for the single crystals and the powders agreed well. Good agreement is also observed with the values reported recently by Iandelli (8), i.e., a = 750.2(1) pm; c = 404.2(1) pm for GdPdMg and a = 767.9(1) pm and c = 418.9(1) pm for GdAgMg.

Single-crystal intensity data of GdAgMg were collected by use of a four-circle diffractometer (Enraf-Nonius, CAD4) with graphite monochromatized MoKα radiation and a scintillation counter with pulse height discrimination. The scans were performed in the $\omega/2\theta$ mode. An empirical absorption correction was applied on the basis of Ψ-scan data. The GdPdMg and GdPtMg crystals were investigated in the oscillation mode on a Stoe image plate system (IPDS) with graphite monochromatized Mo$K\alpha$ radiation. A numerical absorption correction was applied to both

TABLE 1
Crystal Data and Structure Refinement for GdPdMg, GdAgMg, and GdPtMg (Space Group $P\tilde{6}2m$, $Z = 3$)

Empirical formula	GdPdMg	GdAgMg	GdPtMg
Formula weight	287.96 g/mol	289.43 g/mol	376.65 g/mol
Unit-cell dimensions	$a = 750.1(1)$ pm	$a = 768.0(2)$ pm	$a = 738.0(1)$ pm
	$c = 404.10(4)$ pm	$c = 419.92(9)$ pm	$c = 409.02(5)$ pm
	$V = 0.1969\,\text{nm}^3$	$V = 0.2145\,\text{nm}^3$	$V = 0.1929\,\text{nm}^3$
Calculated density (g/cm^3)	7.29	6.72	6.48
Crystal size (μm^3)	$20 \times 20 \times 20$	$20 \times 40 \times 40$	$30 \times 70 \times 70$
Transmission ratio (max/min)	2.64	1.20	2.71
Absorption coefficient (mm^{-1})	31.7	29.7	53.1
$F(000)$	366	369	462
Detector distance (mm)	50	—	50
Exposure time (min)	12	—	6
ϕ range; increment (deg)	0–180; 2.4	—	0–180; 2.0
Profile/pixel	9–25	—	9–25
θ Range for data collection (deg)	3–31	3–30	3–31
Range in hkl	$-9 \le h \le 10, \pm 10, \pm 5$	$-10 \le h \le 2, \pm 10, \pm 5$	$\pm 10, \pm 10, \pm 5$
Total no. reflections	2046	1656	2013
Independent reflections	250 ($R_{\text{int}} = 0.1698$)	261 ($R_{\text{int}} = 0.0844$)	244 ($R_{\text{int}} = 0.1742$)
Reflections with $I > 2\sigma(I)$	234 ($R_\sigma = 0.0784$)	239 ($R_\sigma = 0.0510$)	236 ($R_\sigma = 0.0756$)
Data/restraints/parameters	250/0/14	261/1/16	244/0/14
Goodness-of-fit on F^2	1.105	1.166	1.184
Final R indices [$I > 2\sigma(I)$]	$R1 = 0.0323$	$R1 = 0.0270$	$R1 = 0.0357$
	w$R2 = 0.0685$	w$R2 = 0.0469$	w$R2 = 0.0729$
R indices (all data)	$R1 = 0.0374$	$R1 = 0.0359$	$R1 = 0.0381$
	w$R2 = 0.0703$	w$R2 = 0.0579$	w$R2 = 0.0742$
Flack parameter	$-0.07(4)$	$-0.05(5)$	0.08(4)
Extinction coefficient	0.024(3)	0.016(1)	0.0053(8)
Largest diff. peak and hole (e/Å^3)	1.92 and -1.92	2.07 and -1.28	2.42 and -3.82

data sets. All relevant data concerning the data collections are listed in Table 1.

Magnetic properties of powdered samples were measured with an home-built AC susceptometer associated with the Displex 202 close circle refrigerator operating easily between 12 K and room temperature. Additionally, more precise magnetic investigations were carried out at low temperature (i.e., above 4.2 K and below 150 K) with a Lake Shore 7225 AC Susceptometer/DC Magnetometer. Here, the AC (ACS) and DC magnetic susceptibilities (DCS) as well as the absolute values of the higher harmonics χ_2 and χ_3 were determined as a function of temperature. As a rule, all magnetic measurements were made first using zero-field cooling mode (ZFC), but DC magnetic susceptibilities were also recorded in the field-cooling (FC) mode followed by ZFC. The investigations under ZFC condition were done on heating the sample to 300 K after zero-field cooling to 4.2 K, while the FC measurements were performed on cooling the sample from 300 to 4.2 K in an applied magnetic field of 200 Oe. The field dependence of the magnetization for a given sample was measured at temperatures close to 4.2 K by changing the applied magnetic fields between -55 and 55 kOe starting with the virgin curve obtained after ZFC of the sample.

The ^{155}Gd-Mössbauer experiments with the 86.5 keV gamma transition ($I_g = 3/2$, $E1$, $I_e = 5/2$) were performed with an ordinary transmission-type spectrometer with constant acceleration driving mode at 4.2 K using a standard liquid helium cryostat. The 20 mCi ^{155}Eu source in a $SmPd_3$ matrix was kept in a cryostat at liquid helium temperature. The absorbers with optimized thickness, according to the procedures described in (26, 27), were placed in aluminum containers with thin (0.1 mm) windows to ensure a homogeneous temperature over the sample and also to minimize extra absorption. A 3 cm thick NaI(Tl) scintillation counter was employed for the detection of 86.5 keV gamma rays. Lead plates (i.e., a 0.5 mm Pb plate at the detector and a 0.4 mm Pb plate placed between the source and the absorber) were used to cut off the 105.3 keV gamma line concurrently emitted from the source. The velocity scale was calibrated using a commercial ^{57}Co:*Rh* source with iron foil at room temperature.

Despite the relatively poor resolution, characteristic for ^{155}Gd Mössbauer spectroscopy, the transmission integral formula was applied for fitting the experimental spectra. The resonance-line positions and their relative intensities were calculated by a numerical digitalization routine of the full hyperfine interaction Hamiltonian (28). The interference term described by the factor $\xi = 0.0275$ (29) was

included into the absorption cross-section. The following parameters can be determined from the full analysis of the ^{155}Gd resonance spectra: the isomer shift δ_{is}, the quadrupole interaction constant: $\Delta E_Q = eQV_{zz}/4$, where $Q = (1.30 \pm 0.02)b$ (30), the magnetic hyperfine field H_{hf}, the asymmetry parameter $\eta = (V_{xx} - V_{yy})/V_{zz}$ and the polar angles θ and ϕ, giving the direction of the magnetic hyperfine field with respect to the principal axes of the EFG tensor. During all fits, the source and absorber line widths were constrained to those values previously determined in an independent experiment with a $GdFe_2$ absorber $\Gamma_s = 0.35$ mm/s and the natural width $\Gamma_a = 0.25\,\text{mm}\,\text{s}^{-1}$ (31).

RESULTS AND DISCUSSION

Structure Refinements

Irregularly shaped single crystals of GdPdMg, GdAgMg, and GdPtMg were isolated from the annealed samples by mechanical fragmentation and examined by using a Buerger camera to check their quality for intensity data collection. For the three compounds, the space group $P\bar{6}2m$ was found to be correct during the structure refinements. The relevant crystallographic data are listed in Table 1.

The atomic parameters of CeAuMg (10) were taken as starting values and the three structures were successfully refined using SHELXL-97 (32) (full-matrix least squares on F^2) with anisotropic atomic displacement parameters for all atoms. Refinement of the Flack parameter (33, 34) indicated the correct absolute structure. The enhanced R_{int} values for the GdPdMg and GdPtMg crystals are most likely due to absorption effects.

As a check for the correct composition and the correct site assignment, the occupancy parameters were refined in a separate series of least-squares cycles along with the displacement parameters. With the exception of the magnesium position in GdAgMg, all sites were fully occupied within three standard deviations. The magnesium site of GdAgMg showed a displacement parameter that was too small indicating an enhanced scattering power for this position. This is most likely due to silver/magnesium mixing on the 3*g* position. Transition metal–magnesium mixing has been recently also observed for PrAuMg and HoAuMg (35) and other *RE*AgMg intermetallics (36, 37). Subsequently, we refined this site with a mixed silver/magnesium occupancy resulting in the composition $GdAg_{1.06(1)}Mg_{0.94(1)}$ for the crystal investigated. This site occupancy parameter was refined as a least-squares variable in the final cycles. At first sight, the displacement parameters of the magnesium atoms in GdPdMg and GdPtMg gave no indication for mixed Pd/Mg or Pt/Mg occupancy. Refinements of the occupancy parameters, however, showed values slightly higher than the ideal ones. Subsequent refinements with mixed Pd/Mg and Pt/Mg occupancies resulted in the compositions $GdPd_{1.03(2)}Mg_{0.97(2)}$ and $GdPt_{1.03(1)}Mg_{0.97(1)}$. Since these magnesium sites are fully occupied within three standard deviations, the final cycles were carried out with the ideal values. In view of the high standard deviations, the mixed occupancy is not significant for the palladium and platinum compound. Final difference Fourier syntheses were flat (Table 1). The positional parameters and interatomic distances of the refinement are listed in Tables 2 and 3. Listings of the observed and calculated structure factors are available.[2]

TABLE 2
Atomic Coordinates and Isotropic Displacement Parameters (pm^2) for GdPdMg, GdAgMg, and GdPtMg

Atom	Wyckoff site	*x*	*y*	*z*	U_{eq}
GdPdMg					
Gd	3*f*	0.4137(1)	0	0	95(3)
Pd1	2*d*	$\frac{1}{3}$	$\frac{2}{3}$	$\frac{1}{2}$	106(5)
Pd2	1*a*	0	0	0	123(6)
Mg	3*g*	0.7574(9)	0	$\frac{1}{2}$	117(15)
GdAgMg					
Gd	3*f*	0.4139(2)	0	0	127(3)
Ag1	2*d*	$\frac{1}{3}$	$\frac{2}{3}$	$\frac{1}{2}$	131(5)
Ag2	1*a*	0	0	0	137(6)
Mg	3*g*	0.755(1)	0	$\frac{1}{2}$	223(28)
GdPtMg					
Gd	3*f*	0.4114(2)	0	0	76(3)
Pt1	2*d*	$\frac{1}{3}$	$\frac{2}{3}$	$\frac{1}{2}$	76(3)
Pt2	1*a*	0	0	0	76(4)
Mg	3*g*	0.755(1)	0	$\frac{1}{2}$	67(16)

Note. U_{eq} is defined as one-third of the trace of the orthogonalized U_{ij} tensor. In the GdAgMg crystal, the magnesium site showed a slight mixed occupancy 0.06(1) Ag + 0.94(1) Mg.

Crystal Chemistry and Chemical Bonding

The structures of the intermetallic gadolinium compounds GdPdMg, GdAgMg, and GdPtMg have been refined from single-crystal diffractometer data. The platinum compound is reported here for the first time. Although lattice parameters have been determined for GdPdMg and GdAgMg by Iandelli [8], the precise atomic positions and the small homogeneity range for the silver compound have been established in the present work.

GdPdMg, GdAgMg, and GdPtMg crystallize with the ZrNiAl structure (14–16), a ternary ordered version of the

[2] Details may be obtained from: Fachinformationszentrum Karlsruhe, D-76344 Eggenstein-Leopoldshafen (Germany), by quoting the Registry No's. CSD-412441 (GdPdMg), CSD-412442 (GdAgMg), and CSD-412443 (GdPtMg).

TABLE 3
Interatomic Distances (pm), Calculated with the Lattice Parameters Taken from X-ray Powder Data of GdPdMg, GdAgMg, and GdPtMg

GdPdMg										
Gd:	4	Pd1	303.2(1)	Pd1:	3	Mg	290.1(5)	Mg:	2	Pd2	271.9(5)
	1	Pd2	310.3(1)		6	Gd	303.2(1)		2	Pd1	290.1(5)
	2	Mg	327.6(5)						2	Mg	315(1)
	4	Mg	337.3(1)	Pd2:	6	Mg	271.9(5)		2	Gd	327.6(5)
	4	Gd	391.5(1)		3	Gd	310.3(1)		4	Gd	337.3(1)
	2	Gd	404.1(1)								
GdAgMg										
Gd:	4	Ag1	312.4(1)	Ag1:	3	Mg	296.0(5)	Mg:	2	Ag2	281.7(5)
	1	Ag2	317.9(2)		6	Gd	312.4(1)		2	Ag1	296.0(5)
	2	Mg	336.0(6)						2	Mg	325(1)
	4	Mg	347.4(1)	Ag2:	6	Mg	281.7(5)		2	Gd	336.0(6)
	4	Gd	400.7(1)		3	Gd	317.9(2)		4	Gd	347.4(1)
	2	Gd	419.9(1)								
GdPtMg										
Gd:	4	Pt1	302.5(1)	Pt1:	3	Mg	284.4(5)	Mg:	2	Pt2	272.9(5)
	1	Pt2	303.6(1)		6	Gd	302.5(1)		2	Pt1	284.4(5)
	2	Mg	326.0(6)						2	Mg	313(1)
	4	Mg	334.3(1)	Pt2:	6	Mg	272.9(5)		2	Gd	326.0(6)
	4	Gd	386.0(1)		3	Gd	303.6(1)		4	Gd	334.3(1)
	2	Gd	409.0(1)								

Note. All distances of the first coordination sphere are listed. The magnesium site of GdAgMg shows a slight mixed occupancy of 0.06(1) Ag + 0.94(1) Mg.

Fe_2P type (38). Since the crystal chemistry of ZrNiAl-type compounds has been described in detail in (2, 3, 39, 40), only some relevant details are discussed here. As an example we present the GdAgMg structure in Fig. 1. From a geometrical point of view, the structure is built up from two types of silver centered tricapped trigonal prisms: $[Ag(1)Gd_6Mg_3]$ and $[Ag(2)Mg_6Gd_3]$. The prisms of the Ag1 atoms are condensed via common edges forming larger rings. These are further condensed via common triangular faces. Within these larger rings, the Ag2 centered magnesium prisms are located. The latter are also condensed via the triangular faces.

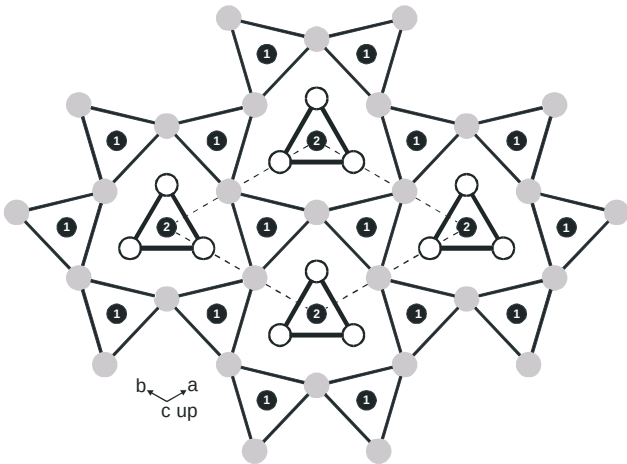

FIG. 1. Projection of the GdAgMg structure onto the *xy* plane. All atoms lie on mirror planes at $z = 0$ and $\frac{1}{2}$, indicated by thin and thick lines, respectively. Gadolinium, silver, and magnesium atoms are drawn as gray, filled, and open circles, respectively. The trigonal prisms around the silver atoms Ag1 and Ag2 are emphasized.

At this point it is interesting to note that the coloring of the various positions by the transition metal and *p* element atoms in the ZrNiAl-type intermetallics depends on the size of these atoms (2, 39, 41). The trigonal prismatic sites are occupied by the smaller atoms. To give an example: In GdAgMg the prisms are filled with the silver atoms ($r_{Ag} = 145$ pm; $r_{Mg} = 160$ pm) while the smaller germanium atoms ($r_{Ge} = 137$ pm) occupy these sites in GdAgGe (42). In most cases this coloring seems to depend on size criteria. In view of the different coloring and thus different chemical bonding, the structures of GdAgMg and GdAgGe should be called isopointal (43, 44) rather than isotypic. The coordination polyhedra for GdAgMg are shown in Fig. 2.

The shortest interatomic distances in GdAgMg occur for the Ag–Mg contacts (282 and 296 pm). These distances are only slightly larger than the sum of Pauling's single bond radii of 270 pm for silver and magnesium (45), indicating bonding Ag–Mg interactions in GdAgMg. The three-dimensional [AgMg] network of the GdAgMg structure is shown in Fig. 3. The gadolinium atoms fill distorted hexagonal channels within this network. This is certainly a simplified view. Each magnesium atom has two magnesium neighbors at 325 pm (triangular face of the

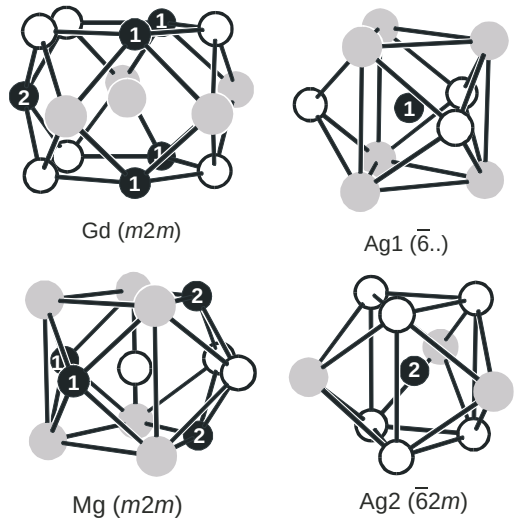

FIG. 2. Coordination polyhedra in the structure of GdAgMg. The two crystallographically different silver sites and the site symmetries are indicated.

prism), only slightly longer than in hcp magnesium (average Mg–Mg distance 320 pm (46)). Thus, also some bonding Mg–Mg interactions might be assumed within the [AgMg] network. In GdPdMg and GdPtMg, the Mg–Mg distances are even shorter than in hcp magnesium.

Finally, we draw back to the comparison of the GdAgMg and GdAgGe structures. The different coloring has a drastic effect on the interatomic distances. The Gd–Ag distances range from 312 to 318 pm in GdAgMg and from 320 to 335 pm in the germanide. An even larger effect is observed for the Gd–Gd contacts: 401–420 pm in GdAgMg and 372–424 pm in GdAgGe (42). The variation of the Gd–Gd distances strongly influences the Gd–Gd coupling and leads to a decrease of the magnetic ordering temperature (being a measure of this coupling) for GdAgGe ($T_N = 13.0(2)$ K) when compared with GdAgMg ($T_C = 39.3(1)$ K).

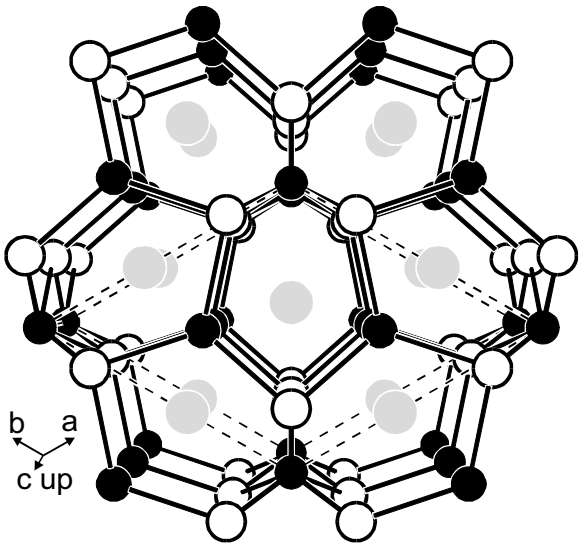

FIG. 3. Perspective view of the GdAgMg structure along the z-axis. Gadolinium, silver, and magnesium atoms are drawn as gray, filled, and open circles, respectively. The three-dimensional [AgMg] network is emphasized.

Bulk Magnetic Properties

The results of the magnetic measurements are shown in Figs. 4–8. The basic magnetic parameters are summarized in Table 4. For all three GdTMg (T = Pd, Ag, Pt) compounds, the real part χ' of the AC susceptibility χ and the inverse susceptibility $1/\chi'$ vs temperature in ZFC mode are shown in Fig. 4. The data are analyzed by the Curie–Weiss law, $\chi = C/(T-\Theta_p)$. By fitting the inverse

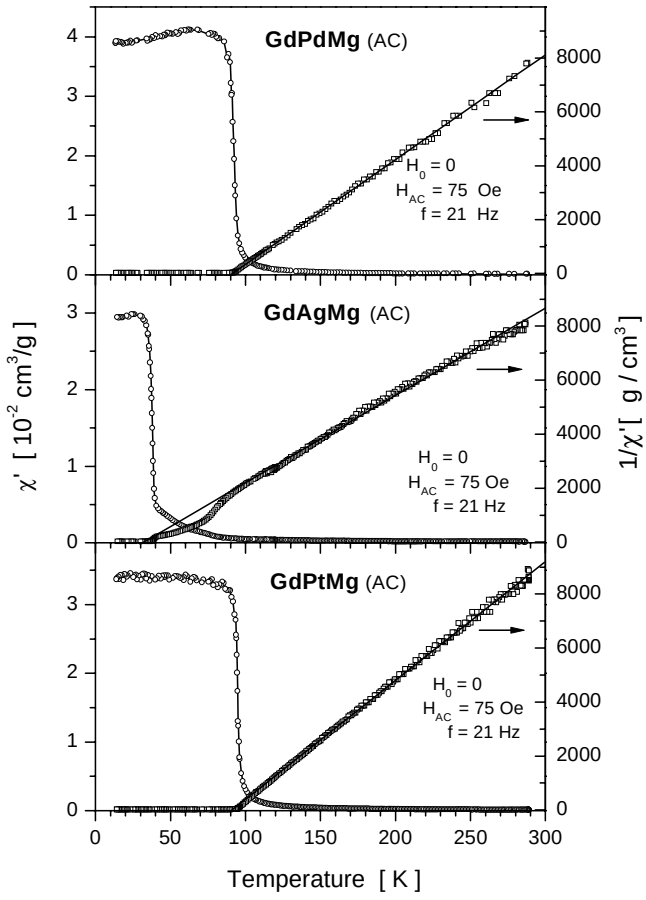

FIG. 4. Overall temperature dependencies of zero-field AC susceptibilities (left-hand scales) and inverse susceptibilities (right-hand scales) as measured for the real part of χ using a home-built susceptometer at an internal frequency $f = 21$ Hz with an oscillating field amplitude $H_{AC} = 75$ Oe. Solid lines shown in the individual figures were obtained for each compound by fits according to the Curie–Weiss law as explained in the text.

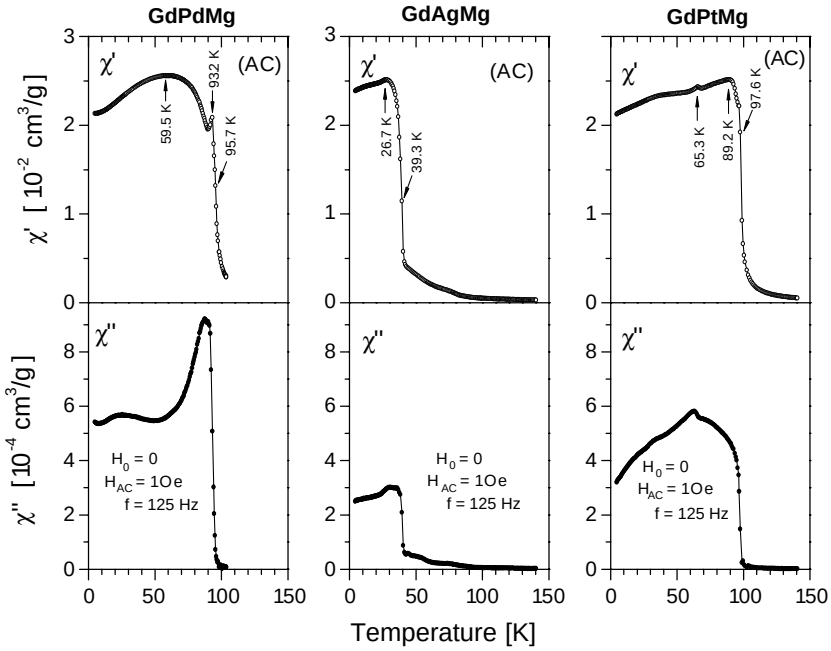

FIG. 5. Low-temperature zero-field susceptibilities $\chi'(\omega)$ and $\chi''(\omega)$ recorded simultaneously as a function of temperature with a Lake Shore 7225 AC susceptometer at an internal frequency $f = 125\,\mathrm{Hz}$ with an oscillating field amplitude $H_{AC} = 1\,\mathrm{Oe}$.

susceptibilities well above the ordering temperatures, the slopes $1/C$ and the individual Θ_p values were obtained (Figs. 4 and 5). The estimated paramagnetic Curie temperatures Θ_p are distinctly positive (Table 4), as is typical for ferromagnets (47). The experimental moments μ_{exp} were derived from the formula $\mu_{exp} = 2.83(MC)^{1/2}$ where M is the molar mass. Their values are very close to the theoretical effective magnetic moment characteristic for free Gd^{3+} ions (ground state $^8S_{7/2}$) $\mu_{eff} = g\,\mu_B[J \times (J+1)]^{1/2} = 7.94\,\mu_B$. Only for GdPdMg the experimental magnetic moment of $\mu_{exp} = 7.66\,\mu_B$ is smaller, while for GdAgMg and GdPtMg the moments are slightly higher, i.e., $\mu_{exp} = 8.05\,\mu_B$ (GdAgMg) and $\mu_{exp} = 8.27\,\mu_B$ (GdPtMg). The excess moments can tentatively be ascribed to a contribution from *d*-electrons mainly of gadolinium, but also of silver and platinum, as already discussed for GdPdCd (18 and references therein).

Detailed ACS and DCS studies performed at low temperatures fully confirmed ferromagnetic transitions. The individual values of these transitions were determined from the inflection points. These correspond to the fastest temperature changes of ACS or DCS curves and they are indicated by arrows in Figs. 5–7. There is good agreement between the AC and DC measurements, since, in fact, the Curie temperature T_C is defined rigorously in zero magnetic field as a temperature where the magnetic order parameter experiences the fastest change vs temperature. T_C results obtained in such a way are reported in Table 4. The magnetic system seems to be independent on the amplitude of the applied AC field ($H_{AC} = 1$ Oe, Fig. 5). A closer inspection of the data displayed in Figs. 5–7 reveals clear maxima (pointed by arrows) observed at the temperature dependencies of $\chi'(T)$ (Fig. 5). They are reflected also at $\chi''(T)$ below the T_C values which can be associated with additional anomalies detected also at the respective dependencies of the second harmonics $\chi_2(T)$ (Fig. 6) as well as with those visible in the $\chi_\sigma(T)$ curves for GdPtMg (Fig. 7) measured in the ZFC and FC mode. These maxima can be ascribed to spin-reorientations, marked by T_{SR} in Table 4, similar to transitions found for pure gadolinium at $T_{SR} = 227\,\mathrm{K}$ and $T_{SR} = 132\,\mathrm{K}$ (48). As for gadolinium (48), all T_{SR} anomalies are reduced upon the application of a magnetic field during DCS measurements which is clearly visible in Fig. 7 where only the first lower temperature anomaly survives on both ZFC and FC curves for GdPtMg.

In analogy with gadolinium, one can assume that for all compounds the easy magnetization axis is primarily parallel to the *c*-axis and lowering the temperature, a spin-reorientation transition takes place. This scenario is supported by the values of the θ angles (Table 5) obtained from ^{155}Gd Mössbauer studies discussed below.

It is generally accepted that non-vanishing values of higher harmonic susceptibilities (χ_2 and χ_3) are a direct signal for the appearance of a spontaneous magnetic moment (49–52). In fact, one observes their non-zero susceptibilities just below T_C, supporting ferromagnetic transitions, as illustrated in Fig. 6. The $\chi_2(T)$

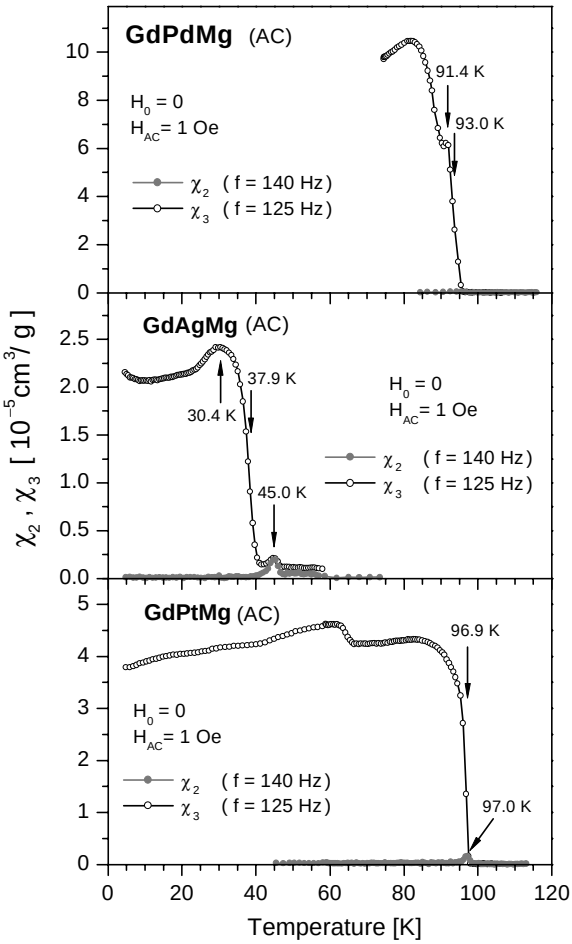

FIG. 6. Temperature dependencies of the signal intensities registered for the second (filled circles) and third (open circles) harmonics χ_2 and χ_3 where the fundamental frequencies were $f = 140$ and $f = 125$ Hz, respectively. Data were collected after ZFC with an oscillating field amplitude $H_{AC} = 1$ Oe.

measurements were performed with a fundamental frequency $f = 140$ Hz to avoid a coincidence of the second harmonic signal with higher harmonics of the power supply current (50 Hz). Additional anomalies (Fig. 6) suggest further magnetic transitions.

Temperature variations of FC and ZFC mass susceptibilities χ_σ measured at a static field $H_0 = 200$ Oe are compared in Fig. 7. A thermomagnetic irreversibility is observed below each individual Curie temperature for every compound. ZFC and FC $\chi_\sigma(T)$ temperature dependencies (Fig. 7) are typical for ferromagnetic materials with temperature-induced magnetic (FM $\leftrightarrow$ PM) phase transitions. They are generally much smoother than the AC susceptibilities (Fig. 5). By cooling a given sample from the paramagnetic state below the Curie temperature in an external field, preferred orientation is induced and therefore the total magnetization is greater than that obtained by ZFC. Insets in Fig. 7 show differences between FC and ZFC mass susceptibilities χ_σ vs temperature, i.e., $[(\chi_\sigma(T))_{FC} - \chi_\sigma(T))_{ZFC}]$. There is excellent agreement between the temperatures of the minima derived from the differences and the temperature determined from the inflection points (Fig. 5). Also, the latter temperatures obtained from ZFC and FC are equal within the experimental errors.

The reason for the magnetic irregularities registered above T_C for GdAgMg (Figs. 4–7) is not obvious since an impurity magnetic phase can be excluded from our X-ray and Mössbauer studies. The maximum developed at 45 K of the second and third harmonics (Fig. 6) might more probably reflect the temperature-induced changes in short-range order magnetic interactions.

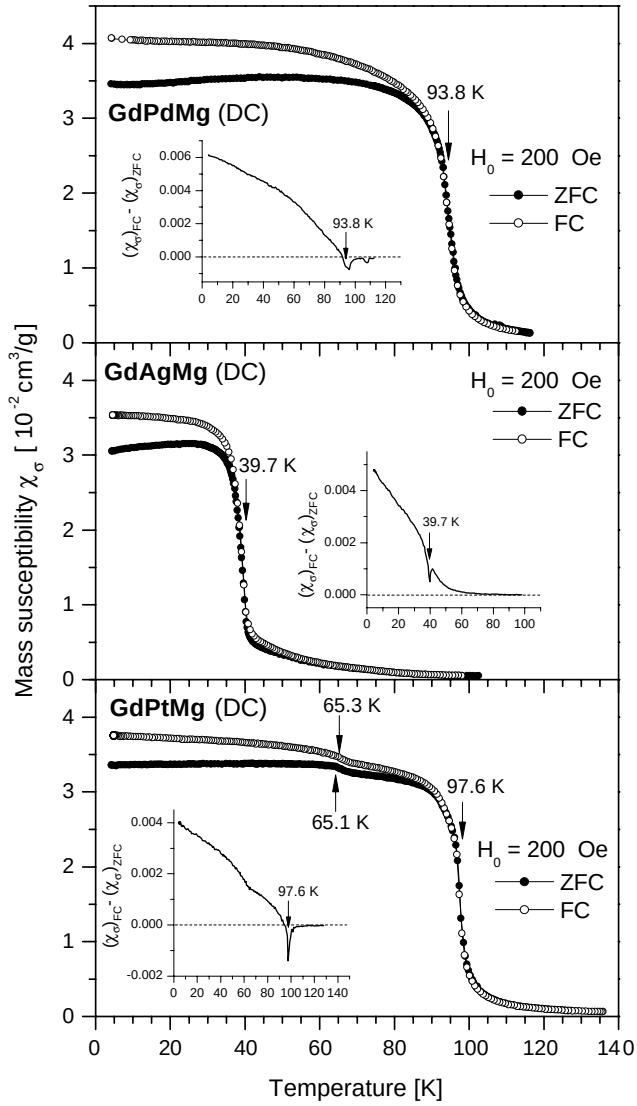

FIG. 7. ZFC and FC DC mass susceptibilities χ_σ measured in a static field $H_0 = 200$ Oe as a function of temperature. Insets show temperature variations of differences between FC and ZFC mass susceptibilities, i.e., $[(\chi_\sigma(T))_{FC} - \chi_\sigma(T))_{ZFC}]$.

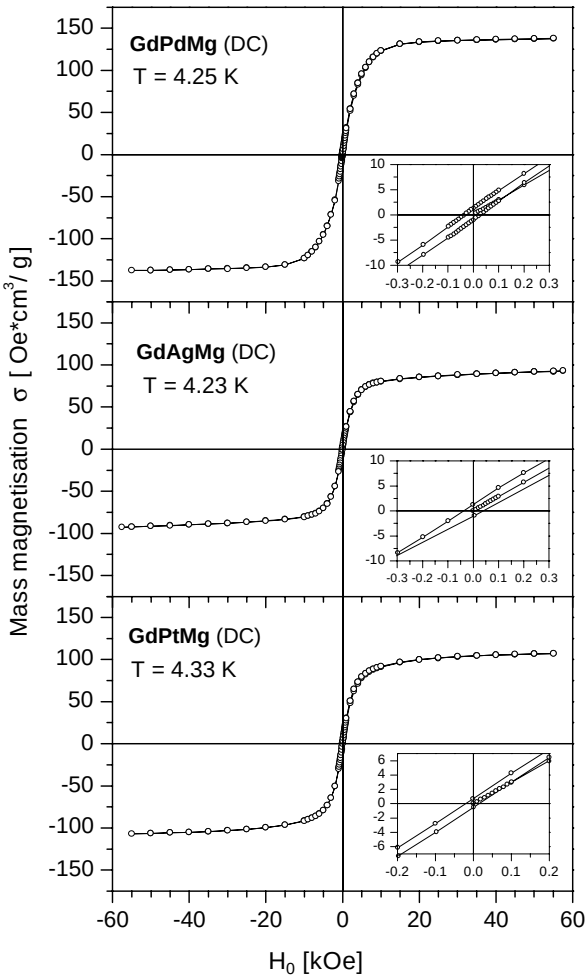

FIG. 8. Hysteresis loops of the mass magnetizations σ measured close to the liquid helium temperature $T = 4.2$ K, which were always started after ZFC of the respective sample. The insets show the enlarged central parts for all samples.

Magnetization measurements carried out in varying magnetic fields from about -55 to 55 kOe at 4.2 K (Fig. 8), points to an apparently soft magnetic behavior of all compounds with small values of the coercive fields H_c and remanent magnetizations σ_r (Table 4). The values of the magnetizations σ obtained at 55 kOe for GdPdMg and GdPtMg lead to 7.10 and 7.22 μ_B/Gd atom, respectively, which compare quite well with the theoretical magnetic moment of 7.0 μ_B/Gd atom and fairly well with the magnetic moment of 7.63 μ_B observed for metallic gadolinium. For GdAgMg, in an even little higher field (57.5 kOe), its magnetization is only 4.82 μ_B/Gd atom.

^{155}Gd Mössbauer Spectroscopy

The resonance spectra measured at 4.2 K for GdPdMg, GdAgMg, and GdPtMg (Fig. 9) clearly demonstrate magnetic hyperfine field splitting. They can effectively be analyzed in terms of a single gadolinium site with a fully mixed electric quadrupole/magnetic dipole interaction Hamiltonian using least-squares fits of transmission integrals (Table 5). In all cases, the fits were insensitive to the value of the tilt angle ϕ, therefore it was fixed at zero. Limited resolution of our ^{155}Gd Mössbauer spectra does not allow determination of the quadrupole interaction signs, although slightly better quality factors χ^2 for fits with positive quadrupole interaction constants were obtained. However, the absolute values were independent of the sign assumed.

The observed isomer shift values δ_{is} (Table 5) makes it possible to compare electron densities at the nucleus site, taking into account the following expression: $\delta_{is} \sim \Delta\langle r^2\rangle_{nucl}$ $(|\psi_a|^2 - |\psi_s|^2)$ where $\Delta < \langle r^2\rangle_{nucl}$ is the difference between the mean-square nuclear radii. $|\psi_a|^2$, $|\psi_s|^2$ denote electron densities (mainly of *s* character) at the nucleus site for the absorber and the source, respectively. For ^{155}Gd the sign of the quantity $\Delta\langle r^2\rangle_{nucl}$ is negative (53), therefore, the smaller the value of δ_{is}, the higher the electronic density $|\psi_a|^2$. Following the results listed in Table 5, we find the lowest electron density in GdAgMg, while higher but comparable densities are observed for GdPtMg and GdPdMg. The values of the electric field gradient V_{zz} at the gadolinium nuclei can be obtained from the quadrupole interaction constants $\Delta E_Q = eQV_{zz}/4$ by the relation: $V_{zz} = 8.8826 \times 10^{21} \Delta E_Q\,(\text{mm/s})\,\text{V/m}^2$.

The local symmetry of the 3*f* gadolinium position with *m*2*m* site symmetry in the ZrNiAl-type structure permits only two possible orientations of the V_{zz}-axis of the EFG tensor, i.e., parallel or perpendicular to the crystallographic *c*-axis. A θ angle is by definition the angle between the

TABLE 4
Magnetic Properties of Gd*T*Mg (*T* = Pd, Ag, Pt) Derived from AC and DC Magnetic Susceptibility Measurements as Described in the Text

Compound	Θ_p (K)	μ_{exp} (μ_B)	T_C (K)	T_{SR} (K)	H_c (Oe)	σ_r (Oe cm^3/g)	σ (μ_B)
GdPdMg	+91(1)	7.66	95.7(1)	93.2(1)	34(2)	1.2(1)	7.10
GdAgMg	+31.9(5)	8.05	39.3(1)	27.6(1)	39(2)	1.2(1)	4.82
GdPtMg	+90.9(5)	8.27	97.6(1)	65.3(1), 89.2(1)	17(4)	0.6(1)	7.22

Note. Θ_p paramagnetic Curie temperature; μ_{exp}: experimental magnetic moment; T_C: Curie temperature; T_{SR}: spin reorientation temperature; H_c: coercive magnetic field; σ_r: experimental mass magnetization; σ: experimental magnetization in units of Bohr magnetons.

TABLE 5
Hyperfine Interaction Parameters Obtained at 4.2 K from the Analysis of ^{155}Gd Mössbauer Spectra for Gd*T*Mg (*T* = Pd, Ag, Pt)

Compound	δ_{is} [a] (mm/s)	ΔE_Q [b] (mm/s)	$\lvert H_{hf}\rvert$ (kOe)	η [c]	θ (deg)	χ^2
GdPdMg	0.192(7)	0.483(9)	212(2)	0.00(15)	80(2)	0.77
GdAgMg	0.272(3)	0.528(5)	214(1)	0.07(3)	60(1)	1.27
GdPtMg	0.190(4)	0.589(6)	188(2)	0.22(7)	46(2)	0.93

[a] Isomer shift; δ_{is} is relative to the (^{155}Eu)SmPd$_3$ source.
[b] Electric quadrupole interaction parameter $\Delta E_Q = eQV_{zz}/4$.
[c] Asymmetry parameter $\eta = (V_{xx} - V_{yy})/V_{zz}$.
For the 86.5 keV gamma transition in ^{155}Gd, 1 mm/s corresponds to $28.868(1) \times 10^{-8}$ eV or 69.803(3) MHz.

V_{zz}-axis and the $\mathbf{H}_{hf}$ vector. Hence, if both directions were parallel to the crystallographic *c*-axis, the θ angle would be zero. This definitely does not go along with the fitting results (Table 5). It means, obviously, that the $\mathbf{H}_{hf}$ vector deviates from the *c*-axis. The refined θ angles are neither 0° nor 90°. This would also be fulfilled if the V_{zz}-axis lies in the basal plane (perpendicular to the *c*-axis) and then in particular, $\mathbf{H}_{hf}$ would be confined in this plane as well.

The magnetic hyperfine field at a nuclear gadolinium site $\mathbf{H}_{hf}$ is usually composed of three terms (54): $\mathbf{H}_{hf} = \mathbf{H}_{CP} + \mathbf{H}_S + \mathbf{H}_N$ where $\mathbf{H}_{CP}$ is the field due to core polarization by the local 4*f* gadolinium moments, $\mathbf{H}_S$ is the self-polarization field due to a polarization of conduction electrons polarized by the local gadolinium magnetic moment, while $\mathbf{H}_N$ is the transferred field contribution of the conduction electron polarization by neighboring magnetic atoms. The absolute value $H_{CP} = -340 \pm 20$ kOe kOe (55, 56) is assumed not to be dependent on the gadolinium environment in solids. The sum $\mathbf{H}_S + \mathbf{H}_N = \mathbf{H}_{CE}$ determines the total field due to conduction electron polarization. It can be calculated as a difference between $\mathbf{H}_{hf}$ and $\mathbf{H}_{CP}$.

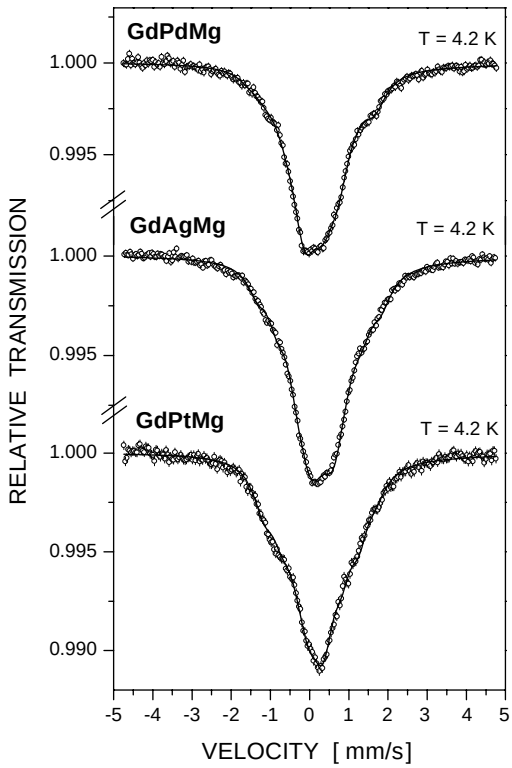

FIG. 9. ^{155}Gd Mössbauer spectra obtained at 4.2 K for Gd*T*Mg (*T* = Pd, Ag, Pt). The continuous lines represent the least-squares fits to the experimental points.

Both, $\mathbf{H}_{CP}$ and $\mathbf{H}_S$, contributions are parallel to the magnetic gadolinium moments. Since for these ferromagnetic compounds gadolinium is the only magnetic component, one can assume in a good approximation that also the structurally related $\mathbf{H}_N$ is parallel to the gadolinium magnetic moments. In this case, the absolute value of H_{CE} can be estimated using the formula: $H_{CE} = H_{hf} - H_{CP}$. Under the assumption that the measured magnetic hyperfine field values H_{hf} (Table 5) are negative, which is usually the case, we can only assume with the above given H_{CP} value that the total contribution of the polarization of the conduction electrons $H_{CE} = H_{hf} - H_{CP}$ is positive for each compound.

Taking all of that into account one can additionally conclude that the net magnetic hyperfine field $\mathbf{H}_{hf}$ should be aligned with the magnetic moment of the gadolinium atoms. Therefore, the deviation of the $\mathbf{H}_{hf}$ vector from the *c*-axis is in accordance with the postulated misalignment of the magnetic gadolinium moments at T_{SR}. The same holds true if the magnetic moment lies within the *ab* plane, in accordance with results deduced from representation theory for the space group $P\bar{6}2m$ (57). The assumed spin reorientation process probably happens between these two possible ferromagnetic spin orientations.

CONCLUSIONS

Three compounds Gd*T*Mg (*T* = Pd, Ag, Pt) have been synthesized as single-phase materials. Their crystal structures and magnetic properties have been investigated by means of X-ray diffraction, AC and DC magnetic

susceptibility measurements as well as ^{155}Gd Mössbauer spectroscopy. The compounds crystallize in the ZrNiAl structure, space group $P\bar{6}2m$. Bulk magnetic measurements carried out in a wide temperature range revealed ferromagnetic transitions for all compounds. Below the Curie temperatures, additional magnetic transitions were observed which are interpreted in analogy to elemental gadolinium to be associated with spin rotation transitions. Except for GdAgMg, the other compounds show excess magnetic moments. Mössbauer spectroscopic results support indirectly the spin-reorientation transitions. The observed full saturation values of the magnetic moments of GdPdMg and GdPtMg might indicate a collinear ferromagnetic structure. The ferromagnetic character of these compounds may be understood in terms of nearest neighbors ferromagnetic coupling. The reduced value of the magnetic moment of GdAgMg can be explained by a non-collinear magnetic structure, meaning antiferromagnetic coupling with the second nearest-neighbors. Preliminary Monte Carlo simulations on GdAgMg suggest that this coupling might lead to frustration, which would explain the anomalous behavior of GdAgMg.

ACKNOWLEDGMENTS

This work was financially supported by the Fonds der Chemischen Industrie and the Deutsche Forschungsgemeinschaft. We are also indebted to the Degussa-Hüls AG for a generous gift of noble metals.

REFERENCES

1. P. Villars and L. D. Calvert, "Pearson's Handbook of Crystallographic Data for Intermetallic Phases," 2nd ed. American Society for Metals, Materials Park, 1991, and Desk Edition, 1997.
2. E. Parthé, L. Gelato, B. Chabot, M. Penzo, K. Cenzual, and R. Gladyshevskii, TYPIX–standardized data and crystal chemical characterization of inorganic structure types, "Gmelin Handbook of Inorganic and Organometallic Chemistry," 8th ed. Springer, Berlin, 1993.
3. E. Parthé and B. Chabot, *in* "Handbook on the Chemistry and Physics of Rare Earths" (K. A. Gschneidner Jr. and L. Eyring, Eds.), Chap. 48. Elsevier Science Publishers, Amsterdam, 1984.
4. A. Szytuła and J. Leciejewicz, "Handbook of Crystal Structures and Magnetic Properties of Rare Earth Intermetallics." CRC Press, Boca Raton, FL, 1994.
5. R. Pöttgen and D. Johrendt, *Chem. Mater.* **12,** 875 (2000).
6. R.-D. Hoffmann and R. Pöttgen, *Z. Kristallogr.* **216,** 127 (2001).
7. M. L. Fornasini and F. Merlo, *J. Alloys Compd.* **219,** 63 (1995).
8. A. Iandelli, *J. Alloys Compd.* **203,** 137 (1994).
9. C. Geibel, U. Klinger, M. Weiden, B. Buschinger, and F. Steglich, *Physica B* **237–238,** 202, (1997).
10. B. J. Gibson, A. Das, R. K. Kremer, R.-D. Hoffmann, and R. Pöttgen, *J. Phys. Condens. Matter* **14,** 5173 (2002).
11. A. Iandelli, *J. Alloys Compd.* **182,** 87 (1992).
12. R. Mishra, R. Pöttgen, R.-D. Hoffmann, D. Kaczorowski, H. Piotrowski, P. Mayer, C. Rosenhahn, and B. D. Mosel, *Z. Anorg. Allg. Chem.* **627,** 1283 (2001).
13. A. I. Horechyy, V. V. Pavlyuk, and O. I. Bodak, *Polish J. Chem.* **73,** 1681 (1999).
14. P. I. Krypyakevich, V. Ya. Markiv, and E. V. Melnyk, *Dopov. Akad. Nauk. Ukr. RSR Ser. A* 750 (1967).
15. A. E. Dwight, M. H. Mueller, R. A. Conner Jr., J. W. Downey, and H. Knott, *Trans. Met. Soc. AIME* **242,** 2075 (1968).
16. M. F. Zumdick, R.-D. Hoffmann, and R. Pöttgen, *Z. Naturforsch. B* **54,** 45 (1999).
17. C. B. Shoemaker and D. P. Shoemaker, *Acta Crystallogr.* **18,** 900 (1965).
18. R.-D. Hoffmann, T. Fickenscher, R. Pöttgen, C. Felser, K. Łatka, and R. Kmieć, *Solid State Sci.* **4,** 609 (2002).
19. F. Canepa, M. L. Fornasini, F. Merlo, M. Napoletano, and M. Pani, *J. Alloys Compd.* **312,** 12 (2000).
20. V. K. Pecharsky and K. A. Gschneidner Jr., *Appl. Phys. Lett.* **70,** 3299 (1997).
21. V. K. Pecharsky and K. A. Gschneidner Jr., *Adv. Cryog. Eng.* **43,** 1729 (1998).
22. K. A. Gschneidner Jr. and V. K. Pecharsky, *Annu. Rev. Mater. Sci.* **30,** 387 (2000).
23. R. Pöttgen, Th. Gulden, and A. Simon, *GIT Labor-Fachzeitschrift* **43,** 133 (1999).
24. R. Pöttgen, A. Lang, R.-D. Hoffmann, B. Künnen, G. Kotzyba, R. Müllmann, B. D. Mosel, and C. Rosenhahn, *Z. Kristallogr.* **214,** 143 (1999).
25. K. Yvon, W. Jeitschko, and E. Parthé, *J. Appl. Crystallogr.* **10,** 73 (1977).
26. G. Czjzek, Kernforschungszentrum Karlsruhe, unpublished.
27. G. J. Long, T. E. Cranshaw, G. Longworth, *Mössbauer Effect Ref. J.* **6,** 42 (1983).
28. W. Kündig, *Nucl. Instrum. Methods* **48,** 219 (1967).
29. Y. Tanaka, D. B. Laubacher, R. M. Steffen, E. B. Shera, H. D. Wohlfahrt, and M. V. Hoehn, *Phys. Lett. B* **108,** 8 (1982).
30. K. Tomala, G. Czjzek, J. Fink, and H. Schmidt, *Solid State Commun.* **24,** 857 (1977).
31. G. Czjzek, Mössbauer spectroscopy of new materials containing gadolinium, *in* "Mössbauer Spectroscopy Applied to Magnetism and Materials Science" (G. J. Long and F. Grandjean, Eds.), Vol. 1, p. 373. Plenum Press, New York, 1993.
32. G. M. Sheldrick, "SHELXL-97," Program for Crystal Structure Refinement, University of Göttingen, 1997.
33. H. D. Flack and G. Bernadinelli, *Acta Crystallogr. A* **55,** 908 (1999).
34. H. D. Flack and G. Bernadinelli, *J. Appl. Crystallogr.* **33,** 1143 (2000).
35. R. Pöttgen, R.-D. Hoffmann, J. Renger, U. Ch. Rodewald, and M. H. Möller, *Z. Anorg. Allg. Chem.* **626,** 2257 (2000).
36. Th. Fickenscher and R. Pöttgen, *J. Solid State Chem.* **161,** 67 (2001).
37. D. Johrendt, G. Kotzyba, H. Trill, B. D. Mosel, H. Eckert, Th. Fickenscher, and R. Pöttgen, *J. Solid State Chem.* **164,** 201 (2002).
38. S. Rundqvist and F. Jellinek, *Acta Chem. Scand.* **13,** 425 (1959).
39. E. Hovestreydt, N. Engel, K. Klepp, B. Chabot, and E. Parthé, *J. Less-Common Met.* **85,** 247 (1982).
40. M. F. Zumdick and R. Pöttgen, *Z. Kristallogr.* **214,** 90 (1999).
41. J. T. Zhao and E. Parthé, *Acta Crystallogr. C* **46,** 2273 (1990).
42. B. J. Gibson, R. Pöttgen, R. K. Kremer, A. Simon, and K. R. A. Ziebeck, *J. Alloys Compd.* **239,** 34 (1996).
43. M. L. Gelato and E. Parthé, *J. Appl. Crystallogr.* **20,** 139 (1987).
44. E. Parthé and M. L. Gelato, *Acta Crystallogr. A* **40,** 169 (1984).
45. L. Pauling, "The Nature of the Chemical Bond and The Structures of Molecules and Crystals." Cornell Univ. Press, Ithaca, NY, 1960.

46. J. Donohue, "The Structures of the Elements." Wiley, New York, 1974.
47. N. W. Ashcroft and N. D. Mermin, "Solid State Physics." Holt, Rinehart and Wilson, New York, 1976.
48. S. Yu. Dan'kov, M. Tishin, V. K. Pecharsky, and K. A. Gschneidner Jr., *Phys. Rev. B* **57,** 3478 (1998).
49. H. Negishi, H. Takahashi, and M. Inoue, *J. Magn. Magn. Mater.* **68,** 271 (1987).
50. T. Hashimoto, A. Sato, and Y. Fujiwara, *J. Phys. Soc. Jpn.* **35,** 81 (1973).
51. S. Chikazawa, C. J. Sandberg, and Y. Miyako, *J. Phys. Soc. Jpn.* **50,** 2884 (1981).
52. T. Sato and Y. Miyako, *J. Phys. Soc. Jpn.* **51,** 1394 (1982).
53. E. R. Bauminger, G. M. Kalvius, and F. E. Wagner, Isomer shifts in the rare earth. *in* "Mössbauer Isomer Shifts" (G. K. Shenoy and F. E. Wagner, Eds.), p. 661. North-Holland Publishing Company, Amsterdam, New York, Oxford, 1978.
54. M. A. H. McCausland and I. S. Mackenzie, "Nuclear Magnetic Resonance in Rare Earth Metals." Taylor & Francis, London, 1980.
55. R. E. Watson and A. J. Freeman, *in* "Hyperfine Interactions" (A. J. Freeman and R. B. Frankel, Eds.), p. 53. Academic Press, New York, 1967.
56. R. E. Gegenwarth, J. I. Budnick, S. Skalski, and J. H. Wernick, *Phys. Rev. Lett.* **18,** 9 (1967).
57. P. Javorský, P. Burlet, V. Sechovský, A.V. Andreev, J. Brown, and P. Svoboda, *J. Magn. Magn. Mater.* **166,** 133 (1997).